Ultralong Stretchable Soft Actuator (US^{2}A): Design, Modeling and Application

Wenbiao Wang[1], Yunfei Zhu[2], Shibo Cai[1] and Guanjun Bao[1*]

Abstract

Actuator plays a significant role in soft robotics. This paper proposed an ultralong stretchable soft actuator (US^{2}A) with a variable and sizeable maximum elongation. The US^{2}A is composed of a silicone rubber tube and a bellows woven sleeve. The maximal extension can be conveniently regulated by just adjusting the wrinkles' initial angle of the bellows woven sleeve. The kinematics of US^{2}A could be obtained by geometrically analyzing the structure of the bellows woven sleeve when the silicone rubber tube is inflated. Based on the principle of virtual work, the actuating models have been established: the pressure-elongation model and the pressure-force model. These models reflect the influence of the silicone tube's shell thickness and material properties on the pneumatic muscle's performance, which facilitates the optimal design of US^{2}A for various working conditions. The experimental results showed that the maximum elongation of the US^{2}A prototype is 257%, and the effective elongation could be variably regulated in the range of 0 and 257%. The proposed models were also verified by pressure-elongation and pressure-force experiments, with an average error of 5% and 2.5%, respectively. Finally, based on the US^{2}A, we designed a pneumatic rehabilitation glove, soft arm robot, and rigid-soft coupling continuous robot, which further verified the feasibility of US^{2}A as a soft driving component.

Keywords Soft robotics, Soft actuator, Pneumatic artificial muscle, Modeling

1 Introduction

Inspired by mollusk, various soft actuators and soft robots were proposed, designed, investigated, and manufactured [1]. Especially in recent years, there has been a worldwide research boom on novel soft actuators, with the rapid progress in smart material science and fast prototyping technology [2].

There are several typical soft actuators, such as fluidic elastomer actuators [3], shape memory alloy actuators [4], pneumatic artificial muscle actuators [5], electroactive polymer actuators, and mixture actuation [6]. The pneumatic artificial muscle actuators are highly believed to be commercially practical in the very near future, which can be classified into contraction-type pneumatic muscle [7] and elongation-type pneumatic muscle [8]. The ever-known first pneumatic muscle is a McKibben-type artificial muscle composed of an internal silicone rubber tube and an external woven net. The typical McKibben-type pneumatic muscle could be improved in two ways. The first is insufficient maximum elongation, and the other is that the maximum elongation is fixed when the initial weaving angle is determined during fabrication. Therefore, if the maximum elongation needs to be adjusted, the external woven net must be reassembled.

Prototypes 7–10 in Table 1 are pneumatic muscles based on the traditional weaving mesh design. As mentioned before, the deformation rate of this kind of pneumatic muscle will not exceed 78%. Researchers have also proposed many new types of pneumatic artificial muscles (As those 1–6 shown in Table 1) to increase

*Correspondence:
Guanjun Bao
gjbao@zjut.edu.cn
[1] Key Laboratory of Special Purpose Equipment and Advanced Processing Technology, Ministry of Education, Zhejiang University of Technology, Hangzhou 310014, China
[2] Beijing Institute of Spacecraft Environment Engineering, China Academy of Space Technology, Beijing 100094, China

Wang *et al. Chinese Journal of Mechanical Engineering*   (2023) 36:13

Page 2 of 12

Table 1 Deformation rates of pneumatic artificial muscles

No	First author	Prototype	Elongation\constriction	Utmost elongation\ shrinkage rate (%)
1	H. D. Yang [9]		Elongation	65
2	K. Han [10]		Elongation	183.3
3	T. Abrar [11]		Elongation	100
4	T. Yukisawa [12]		Elongation	222.5
5	E. W. Hawkes [13]		Elongation	271.9
6	N. Thompson [16]		Constriction	30
7	G. Belforte [17]		Constriction	27
8	H. Al-Fahaam [18]		Elongation and Constriction	15\15
9	A. Al-Ibadi [19]		Elongation	52.5
10	H. Al-Fahaam [20]		Elongation	68.8

elongation and adaptability. Yang et al. [9] and Han et al. [10] designed a muscle connected by hollow paper sacs, which were extended by thrusting compressed air into the sacs. Its maximum elongation rate can reach 183.3%, far greater than those of conventional pneumatic muscles. However, because the capsule structure is not rigid enough when spliced together, the fixed parts need to be attached on both sides, limiting the actuator's length [9, 10]. Abrar et al. [11] designed a novel external woven mesh sleeve whose threads are not interwoven with each other. The braided wire is generally wound around the surface of the silicone trachea, like a compressed spring in the free state. After inflating, the braided wire is stretched like a spring under stress. An elongation rate of 271.9% can be achieved in this way. Although this method can provide an excellent elongation rate, there is no mutual constraint between the braided wires. Therefore, the stability and repeatability of the muscles are consequently low [12, 13]. An elongated pneumatic muscle is also proposed based on a bellows braid design. The longer the bellows stacking length, the greater the elongation. For example, the linear-type rubber muscle

designed by Noritsugu et al. [14] is also a bellows pneumatic muscle. With relatively short bellows, it can only reach maximum elongation of 65%. The bellows pneumatic muscle with a corrugated structure designed by Yukisawa et al. [15] has a long stack length, and its ultimate elongation can reach 350%.

Therefore, it can be seen that the elongation of the pneumatic actuator with bellows depends on the specifications of the external bellows braided net. In this paper, according to the bellows' structural characteristics, various ultralong stretchable soft actuators (US^{2}A) with different ultimate deformation rates are developed based on the corrugated mesh sleeve.

Also, establishing a general and accurate mathematical model for PAM has always been challenging. In terms of application, the fundamental model needs to be established to represent the relationship between the inflated air pressure and the pneumatic muscle's structural variables [21]. Furthermore, the mathematical model could provide a theoretical solution for the design of pneumatic muscles in terms of size optimization and material selection. Tondu et al. [22] assumed that the silicone rubber

tube inside the pneumatic muscles is a linear spring without considering its shell thickness. Although this simplified method contributes to building a static model of pneumatic muscles, its accuracy is poor. This modeling method is similar to that proposed by Chou et al. [8]. Both the modeling methods took the cylindrical shape and zero-wall assumption of the inner rubber tube and the braided casing. Consequently, the model established by this method has a deficiency. The main reason lies in the silicone material's highly nonlinear behavior [23] and the effect of the shell thickness of the silicone rubber tube. Yukisawa et al. [15] also proposed a model based on the conservation of stress for the bellows pneumatic artificial muscle, assuming that the longitudinal and lateral deformations of the pneumatic muscle were linear. However, the actual deformation was not linear, and the tensile stress change of the silicone tube was also observed by experiments. Moreover, there are limitations to the generality of the model obtained by the fitting stress experiment. Therefore, the model needs to be improved. The models proposed in Refs. [25, 26] based on the virtual work principle have high accuracy. However, the model does not reflect the influence of the silicone tube's size (such as the shell thickness of the silicone tube) on the pneumatic muscle performance.

To solve the above problems in modeling, the model established in this paper tried to deal with the nonlinearity of the silicone material, analyze the deformation characteristics of soft components, and establish the relationship between the input air pressure and the output of the developed actuator.

This paper first introduces the mechanism and structural design of US²A, then analyzes and verifies the elongation and variable elongation of the bellows woven sleeve by two groups of comparative experiments. Subsequently, the kinematic models of US²A and soft joints were established and simulated based on the elongation principle of the bellows woven sleeve. The established mathematical models were verified experimentally. According to the model and simulation, the proposed actuator can be optimized in size and material selection for preset functional requirements. Based on US²A, a pneumatic rehabilitation glove, soft arm, and rigid-flexible coupling continuous robot were finally designed to demonstrate the practical feasibility of the proposed soft actuator and its model.

2 Design and Operating Principles of US²A
2.1 Mechanical Design and Fabrication

As shown in Figure 1(a), the US²A is composed of a bellows woven sleeve, a silicone rubber tube (with a Shore hardness of 15°), an airtight end cover (resin), and an air inlet cover (resin). The silicone tube is enveloped by the bellows woven sleeve, and the two ends of the silicone tube and the braided mesh sleeve are installed with air inlet end cover and airtight cover, which are fixed by a nylon cable tie. Figure 1(a) shows the fabricating process of the silicone rubber tube. The curing time of the silicone rubber tube is 2 h at a temperature of 120 °C. The silicone tube's maximum elongation rate can reach almost 480% (as shown in the stress-strain curve in Figure 1(b), which is obtained by a uniaxial tensile experiment). The bellows woven sleeve provides the radial constraint to the inner tube.

Figure 1(b) shows the different lengths of the US²A during inflating. The initial length of US²A is 60 mm. When the air pressure was increased to 0.41 MPa, the US²A reached its maximum elongation of 214 mm when the bellows are fully expanded (with the initial opening angle of bellows as $\theta = 0$).
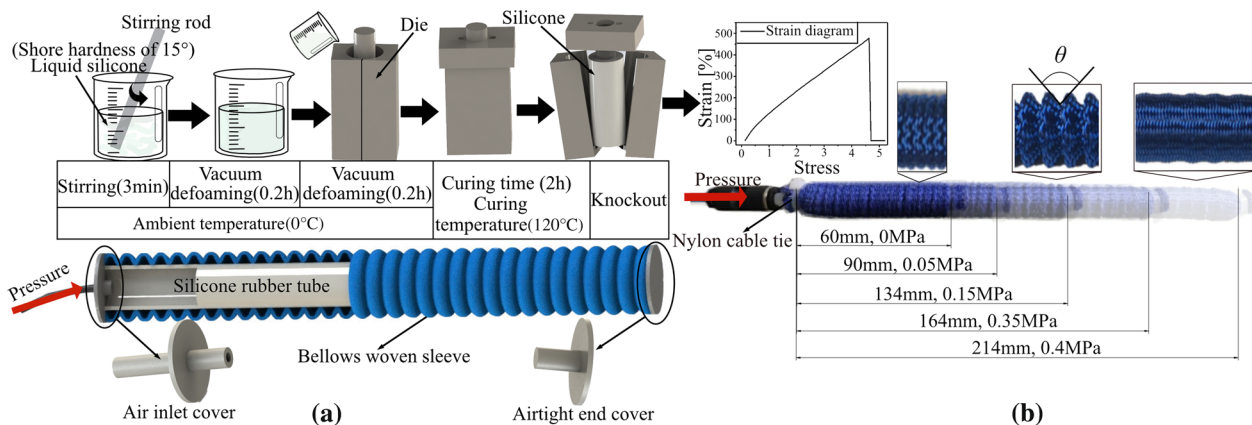

Figure 1 Prototype of US²A: (**a**) fabrication of the rubber tube and partial section view of US²A, (**b**) elongation after inflation

2.2 Variable Maximum Elongation

The initial length of US^2A is determined by the length of the silicone rubber tube, while its maximum length will be determined by the length of the bellows woven sleeve. And the maximum length of the sleeve relies on its number of laps.

Figure 2(a) presents three US^2As with identical bellows laps $n = 30$, whose initial lengths L_0 are 60 mm, 106 mm, and 160 mm, respectively. The three US^2As were inflated with compressed air until reaching their maximum elongation. Figure 2(b) shows the extended length and the corresponding air pressure of the three US^2As, and Figure 2(c) exhibits their elongation rates under different air pressures. The experimental results in Figure 2 show that with the identical bellows laps, the initial length of US^2As is longer, and a lower pressure is required to reach its maximum elongation.

However, the maximum lengths of the three US^2As were the same, suggesting that the maximum elongation of US^2As is determined by the lap number n of its bellows woven sleeve.

In Table 2, Experiment 1 showed the relationship between the maximum elongations and the corresponding pressures. The maximum lengths reached 214 mm, while the corresponding pressures were 0.41, 0.146 and 0.076 MPa, respectively. Therefore, the corresponding elongation rates were 257%, 102% and 33.8%, respectively.

Figure 3(a) and (c) showed the four US^2As with initial lengths L_0 of 106, 106, 160, 160 mm, and corresponding lap numbers n of 53, 30, 80 and 30, respectively. The four US^2As were inflated with compressed air until reaching their maximum elongations. Figure 3(b) and (d) showed the maximum elongation of the four US^2As
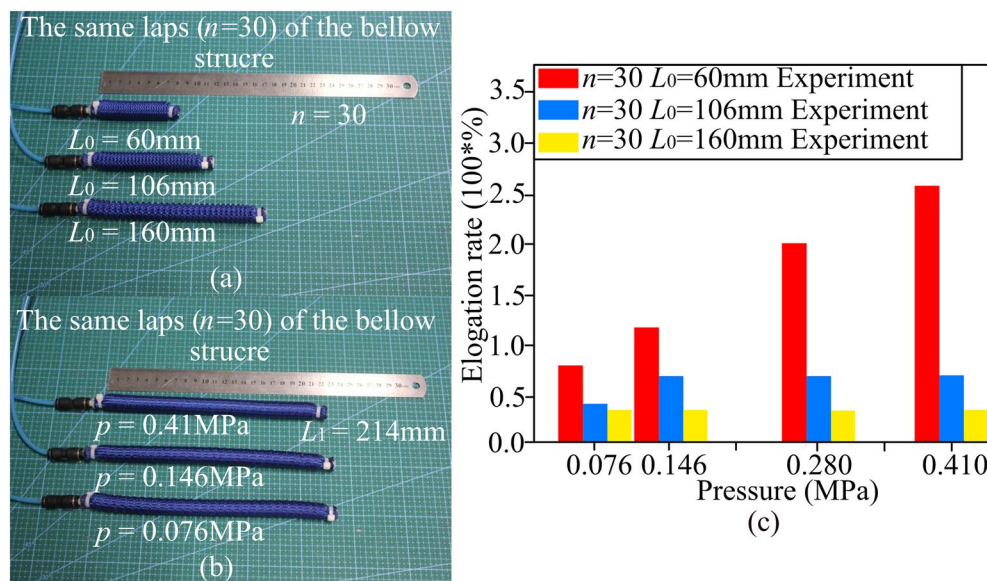

Figure 2 Inflating experiment for US^2A with different initial lengths of the same-lap woven sleeve: (**a**) initial state, (**b**) inflated to the maximum length, **c** stretched rate comparison

Table 2 Deformation rates of US^2As

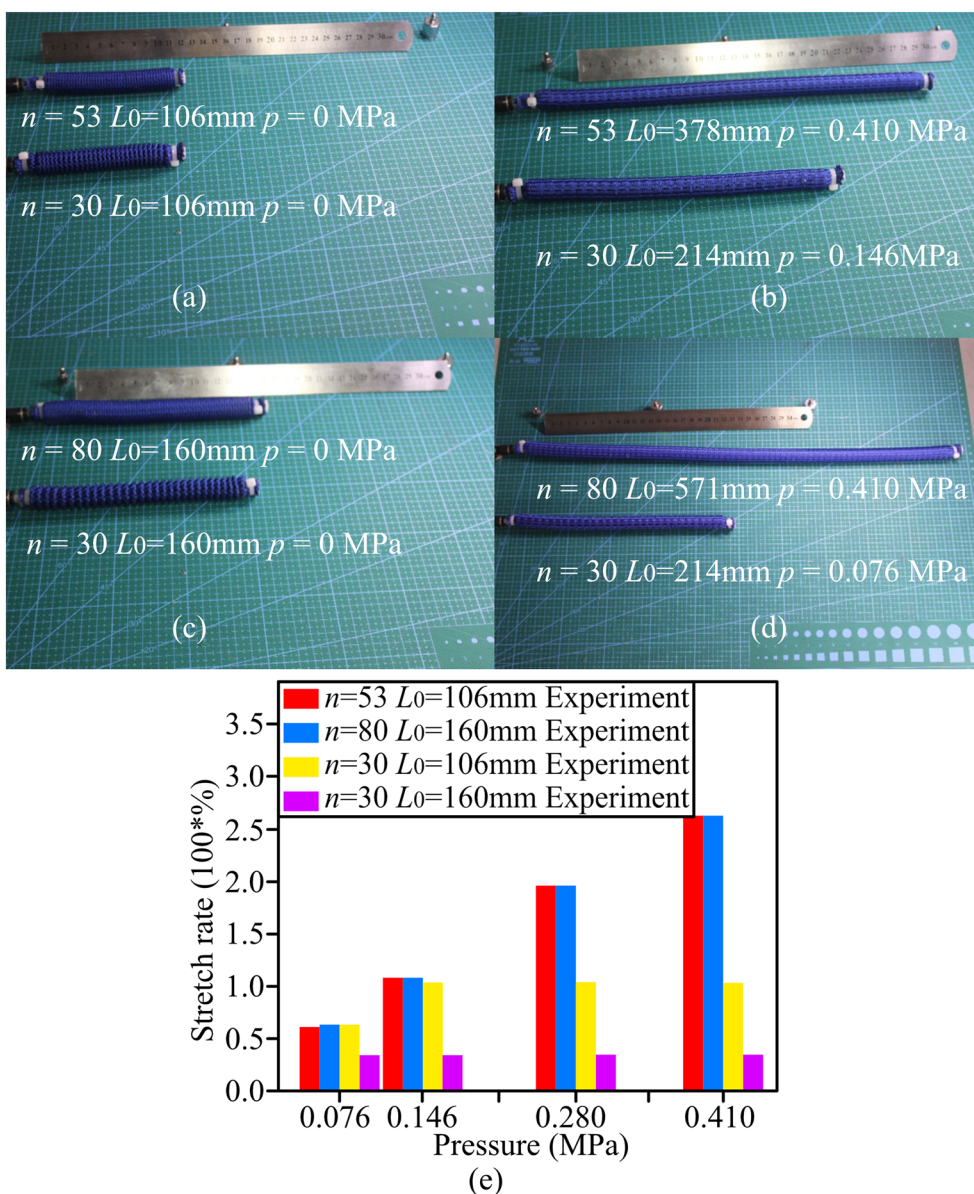|	Initial length (mm)	Bellows coils (*n*)	Corresponding air pressure (MPa)	Maximum length (mm)	Max elongation rate (%)
Experiment 1	60	30	0.410	214.0	257.0
	106	30	0.146	214.0	102.0
	160	30	0.076	214.0	33.8
Experiment 2	106	30	0.146	214.0	102.0
	106	53	0.410	378.5	257.0
	160	30	0.076	214.0	33.8
	160	80	0.410	571.3	257.0

Figure 3 Experimental comparison of US²As with the same initial length while different numbers of bellows laps: (**a**) and (**c**) initial state, (**b**) and (**d**) maximum elongations after inflated, (**e**) stretched rate comparison

and their corresponding air pressures. Experiment 2 in Table 2 provides the maximum elongation rates of the four US²As and their corresponding pressures.

The US²As with an initial length of 106 mm and 53 mm bellows laps reached the maximum length of 378 mm at an air pressure of 0.41 MPa, while the one with an initial length of 160 mm and 80 mm bellows laps reached its maximum length of 571 mm at the same pressure of 0.41 MPa.

Despite their different specifications, the maximum elongation rates of both US²As were 257%. The relationships between the maximum elongation rates of the four US²As and their corresponding air pressures are shown in Figure 3(e). With the same initial length, the more bellows laps US²A has, the longer maximum elongation can be obtained. When the bellows structures of two US²As were entirely compressed at the initial state ($n=53$, $L_0=106$ mm; $n=80$, $L_0=160$ mm), the

corresponding air pressures required for the maximum elongation were the same.

In summary, for the given number of bellows lap (which defines the length of the bellows), the longer the actuator's initial length is, the lower the maximum elongation rates will be, and the lower the corresponding air pressure is required to reach its maximum length. When the initial length of US^{2}A is given, the lower the number of bellows lap is, the lower the maximum elongation rates will be, and the lower the corresponding air pressure is required to reach the maximum length. Moreover, when the bellows were utterly compressed, the corresponding air pressure required to reach the maximum length elongation will be the same.

3 Modeling

3.1 Geometrical Analysis

The section view of US^{2}A is shown in Figure 4(a), where r_0 is the initial inner radius, L_0 is the initial length of US^{2}A and t_0 is the initial thickness of the silicone rubber tube. The initial opening angle bellows are $0° \leq \theta \leq 180°$. When US^{2}A is filled with compressed air, the opening angle θ will increase, and the actuator will extend. We set r_1, t_1, L_1 as the dimensional parameters after inflating, representing the inner radius, the shell thickness of the silicone rubber tube, and the length of US^{2}A, respectively.

As shown in Figure 4(a), before inflating, the bellows structure consists of a semicircle with a diameter of 2 mm and two vertical lines with a length of 2 mm. After inflated, the bellows structure is pushed outward by the silicone rubber tube. The semi-circular profile is expanded into a circular arc with an angle of θ (as shown in Figure 4(b)), and a is the chord length, r is the arc radius, d is the chord height. Furthermore, the express of (r_1, θ) and (L_1, θ) by geometric analysis can be written as:

$$r_1 + t_1 = 2d + 5 + \sin\frac{\theta}{2}, \tag{1}$$

and L_1 and θ can be represented by:

$$L_1 = na + 4n\cos\frac{\theta}{2}, \tag{2}$$

where n is the number of bellows laps.

The silicone rubber tube is taken as incompressible material whose volume will remain constant during deformation ($\pi r_0 t_0 L_0 = \pi r_1 t_1 L_1$). Therefore, both r_1 and L_1 can be expressed by θ:

$$-r_1^2 + r_1 L_1 \left(2d + 5 + \sin\frac{\theta}{2} \right) = r_0 t_0 L_0. \tag{3}$$

For extension-type pneumatic actuators, elongation is the "effective motion", which is expected to be utilized in practice. Simultaneously, the radial movement is a "cost motion", which often consumes energy. From the above mathematical equations, we have axial length L_1, inner radius r_1, and the thickness of silicone rubber t_1 with respect to angle θ. When the axial deformation rate reached 257%, the radius deformation was less than 4 mm. This paper defines the cost motion coefficient (CMC) δ as:

$$\delta = \frac{D}{L}100\%, \tag{4}$$

where D is the radial width of US^{2}A, and L is the axial length of US^{2}A.

Figure 5 shows the simulation result of US^{2}A according to Eq. (3). The relationships between the axial length and radial length of three US^{2}A with the same n and different L_0 were plotted. A small CMC means high efficiency. The CMC of US^{2}A is 3.25% in this paper, which is smaller than that of most pneumatic muscles in Refs. [7,
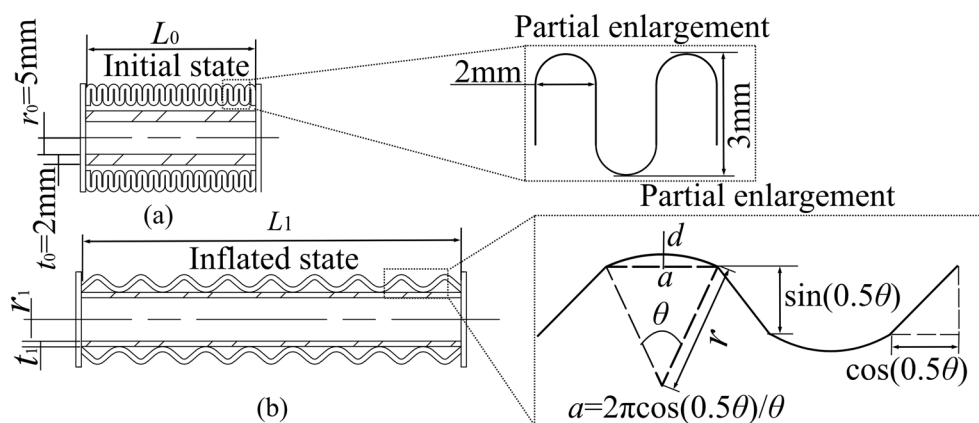

Figure 4 Sectional view of US^{2}A: (**a**) initial state, (**b**) inflated state
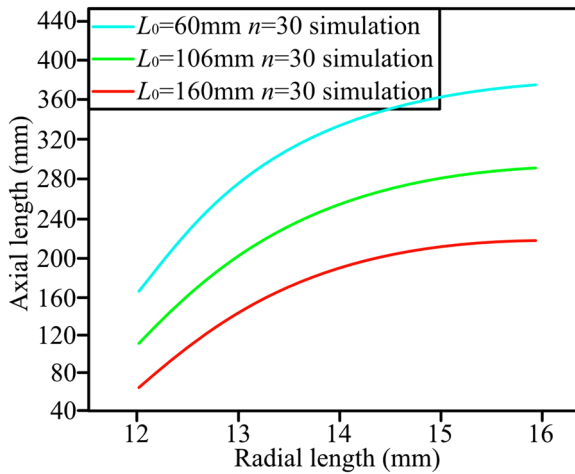
Figure 5 Simulation of axial length and radial length

23–26]. It can also be seen from Figure 5 that the longitudinal elongation and radial elongation of US²A change non-linearly.

3.2 *Static Model of US²A*

A new approach is proposed for determining the relationship between pressure and deformation. According to Yeoh's model, silicone rubber's elastic potential energy can be defined as the product of deformation and strain energy density. The silicone rubber tube is always in static equilibrium after deformation, and the elastic potential energy of the silicone rubber is provided by gas work. In this paper, CMC is determined by the woven sleeve. If CMC is given, the relationship between the air pressure and elongation of US²A can be obtained.

In the deformation processes of US²A, Yeoh's model could be employed to analyze the deformation of silicone material. $\lambda_1 = L_1/L_0$, $\lambda_2 = t_1/t_0$, and $\lambda_3 = 1/(\lambda_1\lambda_2)^{1/2}$ are principal stretches of US²A in three directions. $I_C = \lambda_1^2 + \lambda_2^2 + \lambda_3^2$ is the first Cauchy-Green strain invariant. Variation of strain energy density can be written as:

$$W_C = C_{10}(I_C - 3) + C_{20}(I_C - 3)^2, \qquad (5)$$

where *Wc* is strain energy density; C_{10} and C_{20} are material parameters of silicone rubber measured by strain experiment ($C_{10} = 0.02865$, $C_{20} = 0.00215$ in this paper). The change in silicone rubber's elastic potential energy equals the product of deformation and strain energy density.

$$P_W = \frac{\delta\left(W_C \pi L_1\left((r_1 + t_1)^2 - r_1^2\right)\right)}{\delta\theta}, \qquad (6)$$

$$P_P = \frac{\delta\left(\pi r_1^2 L_1 - \pi r_0^2 L_0\right)}{\delta\theta}, \qquad (7)$$

where δP_W is the elastic potential energy of silicone; δP_P is virtual work done by air pressure; ΔV is internal volume changes; *p* is the air pressure.

Employing principle of virtual work ($\delta P_W = \delta Pp$) and ignoring the friction effect and elastic hysteresis of rubber, we have the relationship:

$$p = \frac{\frac{\delta\left(W_C \pi L_1\left((r_1+t_1)^2 - r_1^2\right)\right)}{\delta\theta}}{\frac{\delta\left(\pi r_1^2 L_1 - \pi r_0^2 L_0\right)}{\delta\theta}}. \qquad (8)$$

Combining Eqs. (1) and (2), W_C and r_1 can be calculated with respect to *θ*. Therefore, Eq. (8) can represent the relationship between the input air pressure *p* and the opening angle *θ* of the US²A bellows.

3.3 *Force Model of US²A*

Combined with the conservation of kinetic energy, the work done by the output force during the motion of the pneumatic actuator can be defined as the work done by the pressure in the silicone rubber minus the change in the potential energy of the silicone material, that is:

$$\int F \mathrm{d}L = \int p \mathrm{d}V - W_C S, \qquad (9)$$

where, d*L* is the axial deformation of US²A; d*V* is the inner volume change; *S* is the volume of pneumatic muscle silicone rubber.

Solving Eq. (9) can get the relationship between US²A output force and air pressure as follows:

$$F = p\left(2\pi r_1 r_1' L_1 + \pi r_1^2\right) - Wc\left[\pi L_1\left((r_1 + t_1)^2 - r_1^2\right)\right]. \qquad (10)$$

4 Model Validation

Figure 6 illustrates the experimental setup for the US²A force test. The US²A is vertically placed in a guide sleeve under a dynamometer (ALIPO-ZP-50) with adjustable height. When inflated, the US²A performed a preset elongation in the guide sleeve, and the dynamometer measured the output force. The inflated US²A is compressed with an increment of 5 mm till to its initial length.

Three US²A prototypes with the same number of bellows laps ($n = 30$) are fabricated with different initial lengths of 60 mm, 106 mm, and 160 mm, respectively. Figure 7(a) shows the experimental and simulated curves of the air pressure and elongation of the three US²As. It can be seen that the experimental results were in good consistency with that of the mathematical model, with an
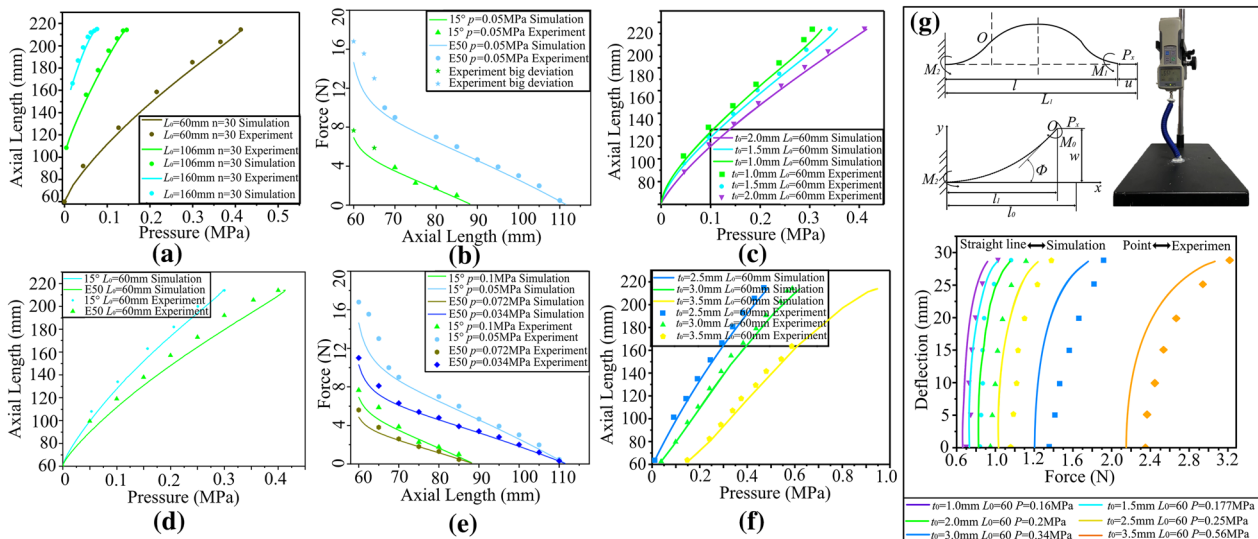
Figure 6 Output force tests of US^{2}A

Figure 7 Experiments and simulation of US^{2}A: (**a**) relationship between elongation and air pressure, (**b**) output force with respect to length under constant air pressure, (**c**) and (**d**) relationship between the air pressure and the elongation of the different shell thicknesses of the silicone tube, (**e**) output force of two different materials US^{2}A, (**f**) relationship between elongation and air pressure of different material US^{2}A, (**g**) US^{2}A buckling strength experiment and simulation

average error of 5% between the model and the experimental data.

As shown in Figure 7(b), the relation between the shape and output forces is represented respectively in simulation and experiment. When the elongation is higher than 10%, the average error is 2.1% in the simulation and experiment, acceptable in the pneumatic muscle's force-variable model. Noticeably, the two-color star point in Figure 7(b) is the output force of experimental data with an elongation of about 10%. It can be seen that the error between the experimental data and the simulated data

exceeds 10%. This happens possibly due to the friction between the bellow woven sleeve and the silicone tube.

To be more specific, when the reverse compression shape variable of pneumatic muscle increases, the friction force also increases, affecting the pneumatic muscle's actual output force. Therefore, to establish a more accurate output force model, the bellows woven sleeve friction with the silicone tube should be considered in the modeling [27].

It should be mentioned that the guide tube in Figure 6 was just employed to provide the track for the actuator

property test. While in most applications, the US^{2}A will not be used in the pipeline.

As shown in Figure 7(b) and (e), for two US^{2}As of the same mechanical specification while with different internal silicone rubber materials, the aforementioned elongation, and output force tests were carried out. As shown in Figure 7(e), the axial output force of US^{2}A made of silicone with different hardnesses differs for the same pressure. Under the same deformation, the greater the hardness of the silicone tube is, the higher the axial output force of US^{2}A will be. Each group of the curves showed the force-length profile of the same US^{2}A under different inside pressures. The curves intersected with each other on the horizontal axis at the free state of elongation. That is, there is no output force. It can be seen from the above experiments that the performance of US^{2}A can be regulated by changing the bellows length and internal silicone rubber material, which can meet demands for different applications.

In order to investigate the influence of the shell thickness of the internal silicone tube of the US^{2}A on its performance, Eqs. (5) and (8) are incorporated into Eq. (7) to eliminate the opening angle θ of the bellows and the pneumatic muscle elongation L_1. Then the relationship between the US^{2}A input air pressure and the silicone tube's shell thickness can be obtained. Figure 7(c) and (d) shows the simulation and experimental comparison diagrams of US^{2}A air pressure and elongation for four kinds of the same length of an internal silicone tube with different shell thicknesses. It can be seen from the figure that the shell thickness of the silicone tube has a significant influence on the performance of the US^{2}A. The thicker the silicone tube's shell thickness inside the US^{2}A, the greater pressure will be required for the same deformation. As shown in Figure 7(d), when the silicone tube's shell thickness is 3.5 mm, the air pressure required for US^{2}A to reach the maximum elongation is 0.96 MPa. The model established in this paper properly describes the relationship between the input air pressure and the various dimensions of the proposed actuator. It provides the theoretical solution for the optimal design of pneumatic muscles.

To further analyze the influence of the shell thickness of the US^{2}A silicone tube on the driving performance, a US^{2}A aerodynamic model and a beam buckling model are established based on Eq. (7). Figure 7(g) shows the buckling experiment after being subjected to the axial load P_x. Point O is the inflection point of the curve. Take 1/4 part of the curve for deflection analysis. The bending stiffness $E(p)I(p)$ of US^{2}A can be expressed as:

$$E(p)I(p) = \frac{\pi p(r_0 + t_0)\left[(2r_1 + 2t_1)^4 - (2r_0 + 2t_0)^4\right]}{64(r_1 + t_1 - r_0 - t_0)}. \tag{11}$$

Incorporating $E(p)I(p)$ into the beam buckling model [28], the axial force and deflection expressions can be obtained:

$$\begin{cases} P_x = \left(\dfrac{\int_0^{\frac{\pi}{2}} \frac{\mathrm{d}\delta_1}{\sqrt{1 - \sin^2(\Phi)\sin^2(\delta_1)}}}{l_1} \right) E(p)I(p), \\[2em] y = \dfrac{2\sin(\Phi)l_1}{\int_0^{\frac{\pi}{2}} \frac{\mathrm{d}\delta_1}{\sqrt{1 - \sin^2(\Phi)\sin^2(\delta_1)}}}, \end{cases} \tag{12}$$

where P_x is the axial output force; l_1 is the 1/4 of the length before buckling in US^{2}A; Φ is the tangent angle at point O; δ_1 is the new variable introduced, and y is the deflection.

The data chart in Figure 7(g) showed the buckling strength analysis of six US^{2}As with the same original length and different shell thicknesses when they reached 150 mm. It can be seen from the experimental data that the axial buckling strength of US^{2}A is meager under different shell thicknesses and air pressure. Taking the US^{2}A with $t_0 = 3.5$ mm as an example, the gas inflation pressure reached 0.56 MPa, while its axial force is only 3.27 N, resulting in a deflection of 28.5 mm. This test showed that the axial buckling strength of US^{2}A is significantly weakened due to its low stiffness.

US^{2}A has different performance requirements in the actual application under different working conditions. The theoretical analysis of Eq. (8), simulations, and experimental data of Figure 7 can be used to facilitate the best size design and silicone material selection for US^{2}A.

5 Application Trials of US^{2}A
5.1 Pneumatic Rehabilitation Glove
As shown in Figure 8(a), a constraint line was embedded in one side of US^{2}A, and it can achieve unidirectional inflection, as shown in Figure 8(b). Based on this derived US^{2}A, a rehabilitation glove was designed and fabricated, as shown in Figure 8(c), which can be used for rehabilitation training of patients with hemiplegia.

5.2 Soft Arm
The soft arm based on US^{2}A is shown in Figure 9, which consists of three sections. The front-end tentacle part comprises three US^{2}As (made of Ecoflex00-50), and each
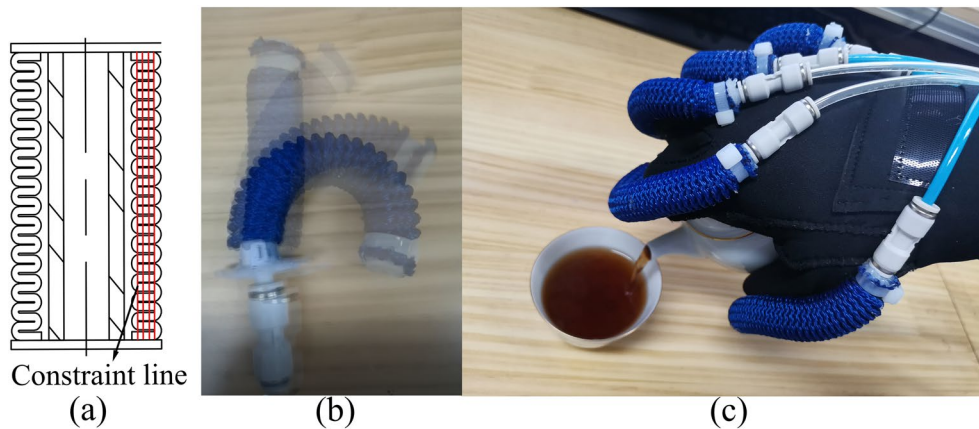
Figure 8 Pneumatic rehabilitation glove: (**a**) sectional view of US²A with a constraint line, (**b**) US²A bend test, (**c**) rehabilitation glove grasping experiment
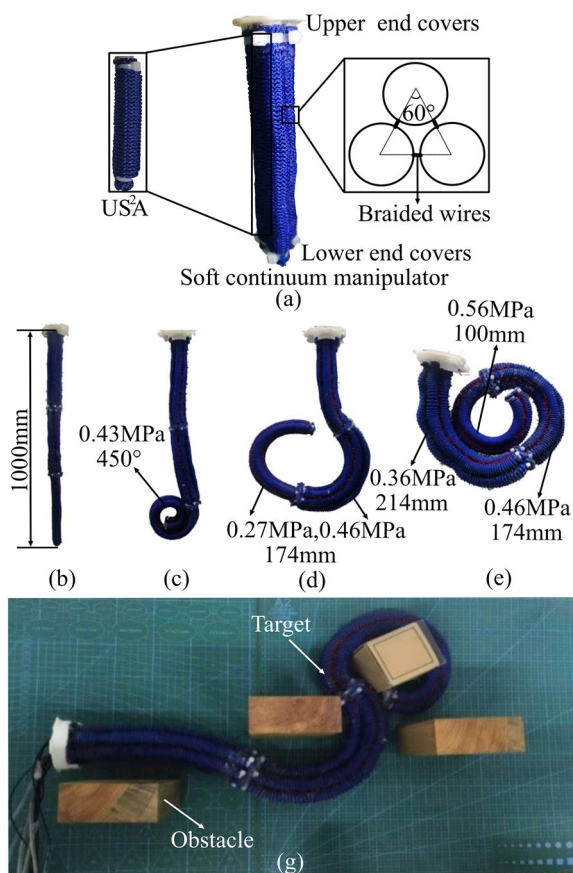

Figure 9 Soft arm based on US²A: (**a**) US²A connection pattern, (**b**) initial state of the soft arm, (**c**) the front end is inflated with 0.43 MPa, (**d**) the front end inflated with 0.27 MPa, and the middle joint inflated with 0.46 MPa, (**e**) the three joints were inflated with 0.36 MPa, 0.46 MPa, and 0.56 MPa, respectively, (**f**) obstacle avoidance and target holding

of the three symmetrically distributed US²As can be independently controlled. Since the other two sections need to take the weight of the front end as load, they were designed with six US²As and fabricated of silicone material with Shore hardness 15°, which could perform powerfully. The two adjacent US²As form a group of the control unit, resulting in three independent controllable channels. The connection structure between US²As is shown in Figure 9(a). The braided wire passes through the inner recess of each corrugated structure and connects them side by side. This connection method will not restrict the extension of US²A and ensure the consistency of its output force transmission.

One of the typical representatives of the pneumatic soft arm robot is the Air-October [29], which has an ultimate elongation rate of 75%. The extension efficiency of various soft arms designed by subsequent researchers is similar to the Oct Arm. Nevertheless, Taigo Yukisawa designed a ceiling continuous arm [12] with a maximum elongation of 280%. However, its bending consistency is poor when it is bent and extended. The soft arm designed in this paper has the characteristics of large elongation (elongation 257%), as well as stable motion ability. The large bending characteristics and bending consistency characteristics of the soft arm make it flexible and controllable for practice.

5.3 Rigid-soft Coupling Continuous Robot

Figure 10 shows a rigid-soft coupling continuous robot designed with the US²As. The rigid-soft coupling continuous robot adopts a modular design. Each drive module is driven by four US²As independently to achieve bending motion in any direction. The reason for choosing US²A as the driver is that it needs to be pre-stretched with large deformation during
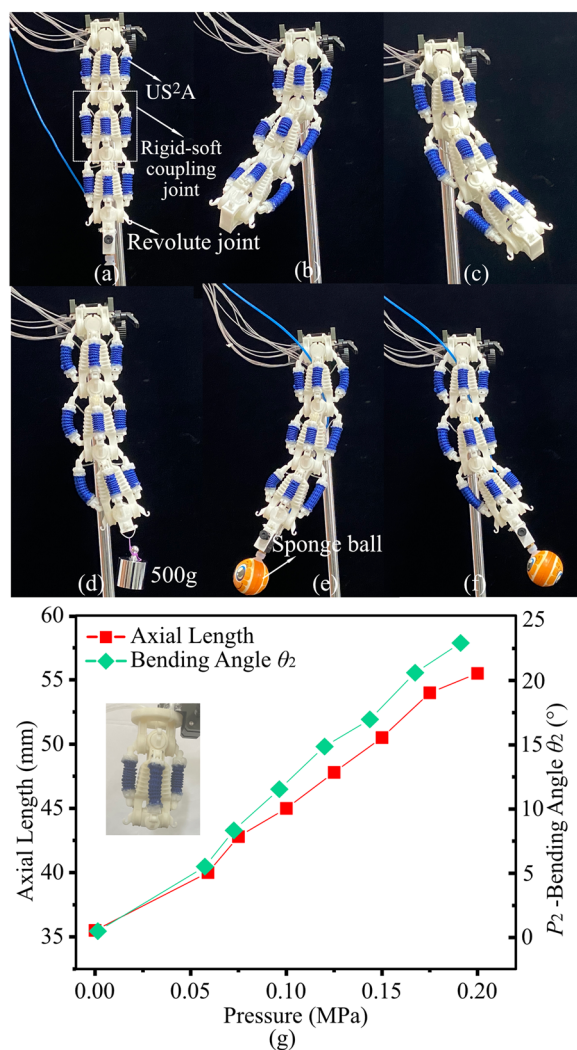
Wang *et al. Chinese Journal of Mechanical Engineering*   (2023) 36:13

Page 11 of 12

Figure 10 Experiments of the rigid-soft coupling continuous robot: **(a)** inflated state, **(b)** and **(c)** space bending motion, **(d)**–**(f)** end load experiment, **(g)** relationship between air pressure, joint bending angle, and muscle elongation

of the rigid-flexible joint, which verified the actuating capability of US^{2}A. In future work, the modeling, characterization, and performance of rigid-flexible coupled continuous robots will be furtherly investigated.

6 Conclusions

(1) This paper presented the design and model of a novel soft actuator US^{2}A. This novel pneumatic artificial muscle actuator exhibits a maximum elongation rate of 257% at relatively low pressure, compared to traditional pneumatic artificial muscles. Moreover, the maximum elongation of the US^{2}A can be conveniently regulated by laps of its bellows sleeve.

(2) Employing the law of energy conservation, a new approach is developed to model the motion and output force of US^{2}A. The established model was further verified by experiments, which also implies that the proposed US^{2}A exhibits a large axial elongation with a small radial deformation. In addition, a mathematical model that defines the relationship between the output force and elongation of US^{2}A was established. The model provides a theoretical basis for designing and optimization of US^{2}A. Three soft robots based on US^{2}A were developed and experimentally verified to prove the feasibility of US^{2}A as a soft actuator.

(3) Still, the proposed US^{2}A has the common shortcoming of low stiffness. Although a soft robot can achieve flexible interaction with the environment, lacking rigidity leads to unstable motion and difficulty in control. In the future, we will design a variable-rigidity skeleton embedded in the US^{2}A to achieve a rigid-flexible-soft structure, which will take the advantages of both soft and rigid robots.

installation. The driver can also have good elongation efficiency after the pre-stretched with large deformation. Therefore, the large deformation characteristics of US^{2}A perfectly adapt to the performance requirements of this robot. The rigid-soft coupling continuous robot spliced by the driving modules can realize the spatial bending motion shown in Figure 10(b) and (c). In addition, Figure 10(d), (e) and (f) showed the load capacity of the rigid-flexible coupling continuous robot.

In this paper, the focus is on the design and performance of the US^{2}A. The practical trials here were just employed to show its potential applications. Figure 10(g) provided the relationship between the air pressure, joint bending angle, and muscle elongation

Author contributions
WW carried out the design of US^{2}A and completed the writing of the paper. YZ proposed the modeling method of US^{2}A. SC conducted experiments and discussion on US^{2}A. GB supervised the investigation and revised the manuscript. All authors read and approved the final manuscript.

Authors' Information
Wenbiao Wang, born in 1993, is currently a Ph.D. candidate at *School of Mechanical Engineering, Zhejiang University of Technology, China*. He received his B.S. degree from *Nanchang Institute of Mechanical Engineering, China* in 2016 and M.S. degree from *Zhejiang University of Technology, China* in 2019. His research interests include soft robot and intelligent robotics.
Yunfei Zhu, born in 1982, is currently a member of *Beijing Institute of Spacecraft Environment Engineering, China*.
Shibo Cai, born in 1981, is currently an associate professor at *College of Mechanical Engineering, Zhejiang University of Technology, China*.
Guanjun Bao (Member, IEEE) born in 1979, received the B.S. degree in mechanical engineering from *North China Electric Power University, Baoding, China*, in 2001, and the Ph.D. degree in mechatronics from the *Zhejiang University of Technology, Hangzhou, China*, in 2006, respectively. He is currently a professor

Wang *et al. Chinese Journal of Mechanical Engineering*　　　(2023) 36:13

Page 12 of 12

with the *College of Mechanical Engineering, Zhejiang University of Technology, China*. His research interests include soft robotics, dexterous hand, and manipulation.

Competing Interests
The authors declare no competing financial interests.

References
[1] G Bao, H Fang, L Chen, et al. Soft robotics: Academic insights and perspectives through bibliometric analysis. *Soft Robotics*, 2018, 5(3): 229–241.
[2] X Wang, R Guo, J Liu. Liquid metal based soft robotics: Materials, designs, and applications. *Advanced Materials Technologies*, 2019, 4(2): 1800549.
[3] M Cianchetti, M Follador, B Mazzolai, et al. Design and development of a soft robotic octopus arm exploiting embodied intelligence. *2012 IEEE International Conference on Robotics and Automation*, *IEEE*. 2012: 5271–5276.
[4] B Tondu, S Ippolito, J Guiochet, et al. A seven-degrees-of-freedom robot-arm driven by pneumatic artificial muscles for humanoid robots. *The International Journal of Robotics Research*, 2005, 24(4): 257–274.
[5] C Laschi, B Mazzolai, V Mattoli, et al. Design of a biomimetic robotic octopus arm. *Bioinspiration & Biomimetics*, 2009, 4(1): 015006.
[6] T E Pillsbury, N M Wereley, Q Guan. Comparison of contractile and extensile pneumatic artificial muscles. *Smart Materials and Structures*, 2017, 26(9): 095034.
[7] F Daerden D Lefeber. The concept and design of pleated pneumatic artificial muscles. *International Journal of Fluid Power*, 2001, 2(3): 41–50.
[8] C P Chou, B Hannaford. Measurement and modeling of mckibben pneumatic artificial muscles. *IEEE Transactions on Robotics and Automation*, 1996, 12(1): 90–102.
[9] H. D. Yang, B. T. Greczek, A. T. Asbeck. Modeling and analysis of a high-displacement pneumatic artificial muscle with integrated sensing. *Frontiers in Robotics and AI*, 2019, 5, 136.
[10] K Han, N H Kim, D Shin. A novel soft pneumatic artificial muscle with high-contraction ratio. *Soft Robotics*, 2018, 5(5): 554–566.
[11] T Abrar, F Putzu, J Konstantinova, et al. Epam: Eversive pneumatic artificial muscle. *2019 2nd IEEE International Conference on Soft Robotics (RoboSoft)*. *IEEE*, 2019: 19–24.
[12] T Yukisawa, S Nishikawa, R Niiyama, et al. Ceiling continuum arm with extensible pneumatic actuators for desktop workspace. *2018 IEEE International Conference on Soft Robotics (RoboSoft)*. *IEEE*, 2018: 196–201.
[13] E W Hawkes, D L Christensen, A M Okamura. Design and implementation of a 300% strain soft artificial muscle. *2016 IEEE International Conference on Robotics and Automation (ICRA)*, *IEEE*. 2016: 022–4029.
[14] T Noritsugu, H Yamamoto, D Sasakil, et al. Wearable power assist device for hand grasping using pneumatic artificial rubber muscle. *SICE 2004 Annual Conference, IEEE*. 2004(1): 420–425.
[15] T Yukisawa, Y Ishii, S Nishikawa, et al. Modeling of extensible pneumatic actuator with bellows (epab) for continuum arm. *2017 IEEE International Conference on Robotics and Biomimetics (ROBIO)*, *IEEE*. 2017: 2303–2308.
[16] N Thompson, X Zhang, F Ayala, et al. Augmented joint stiffness and actuation using architectures of soft pneumatic actuators. *2018 IEEE International Conference on Robotics and Automation (ICRA)*, *IEEE*. 2018: 1533–1538.
[17] G Belforte, G Eula, A Ivanov, et al. Presentation of textile pneumatic muscle prototypes applied in an upper limb active suit experimental model. *The Journal of the Textile Institute*, 2018, 109(6): 757–766.
[18] H Al-Fahaam, S Nefti-Meziani, T Theodoridis, et al. The design and mathematical model of a novel variable stiffness extensor-contractor pneumatic artificial muscle. *Soft Robotics*, 2018, 5(5): 576–591.
[19] A Al-Ibadi, S Nefti-Meziani, S Davis. Design, implementation and modelling of the single and multiple extensor pneumatic muscle actuators. *Systems Science & Control Engineering*, 2018, 6(1): 80–89.
[20] H Al-Fahaam, S Davis, S Nefti-Meziani. The design and mathematical modelling of novel extensor bending pneumatic artificial muscles (ebpams) for soft exoskeletons. *Robotics and Autonomous Systems*, 2018, 99: 63–74.
[21] D Rus, M T Tolley. Design, fabrication and control of soft robots. *Nature*, 2015, 521(7553): 467–475.
[22] B Tondu, P Lopez. Modeling and control of mckibben artificial muscle robot actuators. *IEEE Control Systems Magazine*, 2000, 20(2): 15–38.
[23] E G Hocking N M Wereley. Analysis of nonlinear elastic behavior in miniature pneumatic artificial muscles. *Smart Materials and Structures*, 2012, 22(1): 014016.
[24] D Trivedi, A Lotfi, C D Rahn. Geometrically exact models for soft robotic manipulators. *IEEE Transactions on Robotics*, 2008, 24(4): 773–780.
[25] S H Sadati, S E Naghibi, A Shiva, et al. A geometry deformation model for braided continuum manipulators. *Frontiers in Robotics and AI*, 2017, 4: 22.
[26] M Doumit, J Leclair. Development and testing of stiffness model for pneumatic artificial muscle. *International Journal of Mechanical Sciences*, 2017, 120: 30–41.
[27] M. D Grissom, V Chitrakaran, D Dienno, et al. Design and experimental testing of the octarm soft robot manipulator. *Unmanned Systems Technology VIII*, 2006, 6230: 491–500.
[28] I A Gravagne, I D Walker , C D Rahn. Large deflection dynamics and control for planar continuum robots. *18th Biennial Conference on Mechanical Vibration and Noise Pt.B Clemson University Dept*, 2001: 29634.
[29] W McMahan, B A Jones, I D Walker. Design and implementation of a multi-section continuum robot: Air-octor. *2005 IEEE/RSJ International Conference on Intelligent Robots and Systems. IEEE*, 2005: 2578–2585.